NRIAG Journal of Astronomy and Geophysics 7 (2018) 361–376

Contents lists available at ScienceDirect

NRIAG Journal of Astronomy and Geophysics

journal homepage: www.elsevier.com/locate/nrjag

Full length article

Delineation potential gold mineralization zones in a part of Central Eastern Desert, Egypt using Airborne Magnetic and Radiometric data

Sayed Omar Elkhateeb, Mahmoud Ali Gaballah Abdellatif*

Geology Department, Faculty of Science, South Valley University, Egypt

ARTICLE INFO

Keywords:
Aeromagnetic data
Aeroradiometric data
Structural complexity
Mineralization

ABSTRACT

Localization of probable gold mineralization zones in a selected part of the central Eastern Desert of Egypt has been executed by mapping lithology, structures and hydrothermal alteration zones. In this regard, both aeromagnetic and aeroradiometric data have been utilized in the analysis; by making use of some enhancement techniques such as first vertical derivative, analytic signal and both Center for Exploration Targeting (CET) grid and porphyry. Also, ratio and ternary radiometric maps have been launched to aid in the interpretation process. The results indicated that the study area is dominant by NW, NNW, NNE, WNW, NE, E-W and N-S structural directions. The NW-SE was the most important one and considered as the preferred orientation of ore deposits. Favorable regions of ore deposits were mapped and correlated well with known gold occurrences in the study area beside predicting new zones of mineralization. Analysis of aeroradiometric maps facilitates the correlation and delineation of lithological units based on the concentration of radioelements and ratios. Also, A number of hydrothermal alteration zones were mapped within younger granite, Hammamat felsites and Metasediments. Finally, A composite map consists of geology, structures and hydrothermal altered zones was generated using ArcGIS. Eight known locations of gold mineralization were investigated on this map and also new sites were suggested to be favorable locations for mineralization emplacement.

1. Introduction

The eastern desert of Egypt is considered one of the richest areas of mineral resources, with more than 120 known gold deposits and occurrences (El Ramly et al. 1970). These gold deposits can be categorized into three types stratabound, non-stratabound (most common) and placer gold deposits (Botros, 2004). The non-stratabound deposits are found in the form of vein type mineralization or as disseminated mineralization hosted in volcanics and volcanoclastic rocks (ex: Sukari, Wadi Allaqi, Abu Marawat, Atalla, El-Sid and Atud gold mines). The gold at Sukari, Wadi Allaqi and Abu Marawat areas is hosted in quartz veins parallel to a deep-seated NW-SE to NNW-SSE shear zones. While at Atud, El-Sid and Atalla area, it is hosted in NE-SW veins parallel to a shallow shear zone but at the conjugate point with a deep-seated NW-SE shear zone.

A new tectonic model was proposed for non- stratabound gold deposits (Abu-Alam et al. 2013). This model stated that the gold was deposited from hydrothermal solutions which were produced in a deeper crustal level due to metamorphic or magmatic processes or combination of both. Despite the large number of places and studies carried out in the eastern desert, most of these areas are not exploited well as mining gold is costly and difficult. Also, Gold deposits are hard to find and delineate because gold typically occurs in very low concentrations. Thus, this paper distinguishes the efficiency and accuracy of some convenient and inexpensive geophysical methods which play important role in the investigation and the exploration of ore deposits such as gold, copper and other metal deposits. In this study, we used aeromagnetic and aeroradiometric methods to determine possible location of gold mineralization via delineating structure, mapping lithology and hydrothermal alteration zones.

The role of aeromagnetic method in mineral exploration varies from delineation structures like faults, folds, contacts, shear zones and intrusions to automated detection of porphyry and favorable areas of ore deposits. These structures play important roles in the localization of mineralization. There are various enhancement techniques that can help achieve objectives. These include Horizontal gradient magnitude "HGM" (Cordell and Grauch, 1985), Tilt derivative "TDR" (Miller and Singh, 1994), A directional filter (Cooper, 2003), Theta derivative (Wijns et al. 2005) and normalized standard deviations "NSTD" (Cooper and Cowan, 2008). Also, there are automated methods that can locate

Peer review under responsibility of National Research Institute of Astronomy and Geophysics.
* Corresponding author.
E-mail addresses: sayed.hassan@sci.svu.edu.eg (S.O. Elkhateeb), m.ali@sci.svu.edu.eg (M.A.G. Abdellatif).

https://doi.org/10.1016/j.nrjag.2018.05.010
Received 17 January 2018; Received in revised form 25 May 2018; Accepted 26 May 2018
Available online 01 June 2018

porphyry magnetic signatures and delineate lineaments that used to identify favorable areas of ore deposits (Macnae, 1995; Holden et al. 2008; Core et al. 2009).

On the other hand, Gamma-ray spectrometry measures the surface distribution of naturally occurring radioelements (k, Th, U). These measurements can be used to map and characterize the different lithological units' due to the variation in the concentration of these radioelements between different rocks (Andrson and Nash, 1997; Graham, 1993; Jaques et al. 1997; Charbonneau et al. 1997). In comparison with other airborne geophysical methods, gamma-ray spectrometric method show more success in mapping surface geology (Darnley et al., 1989). Several case studies were conducted in the terms of remapping lithological units by using this technique; (e.g. EI-Meliegy et al. 2000; El-Sadek et al. 2002; Elawadi et al. 2004; Nigm and Khameis, 2009; Youssef and Elkhodary, 2013; Patra et al. 2016). In addition, it is helpful in deducing some structures that may not be recognized through analyzing potential field methods. Also, this method is more useful and accurate in the identification of hydrothermal alteration zones and their detection. Shives et al. (1997) recommend the use of eTh/K ratio as the best indicator of recognizing potassic alteration zones. Thus, many studies were conducted for identifying alteration zones (e.g. Irvine and Smith, 1990; Feebrey et al. 1998; Morrell et al. 2011; Wemegah et al. 2015).

The study area investigated by several researchers such as EI-Bouseily, (1985) who studied Ore-microscopic and geochemical characteristics of gold-bearing sulfide minerals, El Sid Gold mine. Osman and Taman (1996), studied the geology and mineralization of wadi Atalla area. Abd El Rahim et al. (2013) studied Gold-bearing sulfides associated with the granitic wall rock alterations at the Fawakhir area. Akawy (2009), studied the Structural elements and incremental strain history of the basement rocks of Um Had area. Abd El Nabi (2013), clarify the Role of x-ray spectrometry in detecting potassic alteration associated with Um Ba'anib granitic gneiss and metasediments, G. Meatiq area. El-Magd et al. (2015) delineated the lithology, the structural patterns and the alteration zones related to gold mineralization at the Fawakhir area by using advanced space thermal emission and reflection radiometer (ASTER) images.

2. Geological outlines

2.1. location and topography

The area of study represents a part of the Central Eastern Desert, Egypt. It covers approximately 2000 km^2 and bounded by latitudes 25°55′00″ to 26°16′00″N and longitudes 33°15′00″ to 33°5100″ E as shown in Fig. 1a.

The area is mainly occupied by basement rocks of relatively high rugged mountains with many prominent peaks, mostly formed of volcanic and granitic rocks. These rocks are flanking by the phanerozoic sedimentary cover to the west and appear as less rugged and less complex Fig. 1b. Analysis of digital elevation model (DEM) of SRTM data Fig. 2 of the study area showed that the variations in topography range from 56 to 1100 m. The most elevated areas encountered in G. Meatiq (~1110 m), G. Umm Ba′anib (~1040 m), G. El Rubshi (~995 m), G. Atalla (~825 m), G. Murr (~780 m), G. Umm Had (~595 m).

2.2. Geological setting

The Central Eastern Desert can be characterized as mostly occupied by a complex association of metasediments, metavolcanic, Metagabro, and serpentines, constituting the ophiolitic mélange of Shackleton et al. (1980) that is interrupted by gneisses in structural highs. This consequence is unconformably overlain by unmetamorphosed intermediate to silicic volcanic (Dokhan volcanic) and molasse facies clastic sediments (Hammamat clastics). The whole pile is intruded by a vast array of granite intrusions ranging in composition from quartz diorite to alkali- feldspar granite.

Based on the geological map (Fig. 1b) the basement rocks in the studied area occupy the eastern part include metagabbro-metadiorite rocks which comprises metagabbro, gabbro, pyroxenites and cropping out at W. Abu-Diwan, Southeast G. Meatiq. Field studies revealed that the ophiolitic serpentines always have tectonic contacts with the adjoining rocks and that there is an apparent lack of thermal effects. The ophiolitic serpentines located at north G. Meatiq while the talc carbonates occur as separate bodies or as lentoid layers in the ophiolitic ultramafic rocks (El-Mezayen et al. 1995). The hammamat clastics are largely composed of molasses-facies clastic sediments that are intercalated with minor impure calcareous beds as well as Dokhan Volcanics. Post-hammamat felsites are intruded into the hammamat clastics, e.g. at the southwest of Gebel Meatiq. Ultramafic, metavolcanics, and metasediments rocks are exposed in several locations such as around G. Meatiq, Umm Had, G. Umm Anab and G. El Rubshi. The calc-alkaline granites had many terms such as older granites, gray granites, G1 and Gα (El Gaby and Greiling, 1988) granites. The Dokhan volcanic are located at Wadi Abu Diwan and are often associated with the molasse-type sediments and Hammamat ones. Phanerozoic sediments belong to different formations and different ages including Cretaceous sediments (Quseir and Taref Formations) as well as Quaternary deposits.

2.3. Structure

Faults, fractures and shear zones are the main structural features of the study area. These including thrust faults trending NW – SE direction (Gulf of Suez or Red Sea trend), NE-SW fractures which correlate Gulf of Aqaba trends. Normal faults and fractures mostly trending ENE – WSW, NNW – SSE (Stern et al. 1985). Habib (1987), has recognized three orogenic deformations; Meatiqian (affected the ancient Nile craton (Gass, 1977). Abu Ziran (acting along NW – SE compression Trend) and Abu Diwan orogenies (responsible for the NNW – SSE oriented fractures). Other trends such as N – S, E – W are less frequent.

A general outlook of the rose diagram constructed from the geological map modified after Conoco (1987), Fig. 1b indicates that the study area has four main tectonic trends that are oriented along NW-SE, NE-SW, NNE-SSW, and NNW-SSE with minor traces of E-W trend. The area under study is extremely fractured and still subject to tectonic reactivation due to the tectonics of the Red Sea.

2.4. Mineralization

In most cases, gold occurrence is limited to quartz veins taking up pre-existing features and are made up of massive quartz with disseminated gold and sulfides minerals. The country rocks hosting mineralized veins are varied and include serpentinized ultramafics, metamorphosed volcanic and sedimentary rocks, intrusive gabbro and granitoid rocks. Fig. 3a and b represent location map of the gold mineralization occurrences in the study area. This map modified from the mineral map of Egypt, scale 1: 2,000,000 published in 1994 by the Egyptian geological survey and Mining Authority. The study area containing a few old mining. Atalla gold mine area which is situated at about 22 km NNW of the mouth of W. Atalla, at the intersection of lat. 26°9′16″N and long. 33°30′15″ E, it covers about 4 km^2. El Sid and Fawakhir gold mines are located at 93 km due to west from Quseir on the Red Sea coast, along with the Quseir – Qift highway in the Central Eastern Desert of Egypt.

3. Airborne geophysical data

The main data used in this study was a part of the airborne survey conducted by Aero-Service Division, Western Geophysical Company of Aero Service (1984) for the Egyptian General Petroleum Corporation (EGPC) and the Egyptian Geological Survey and Mining Authority

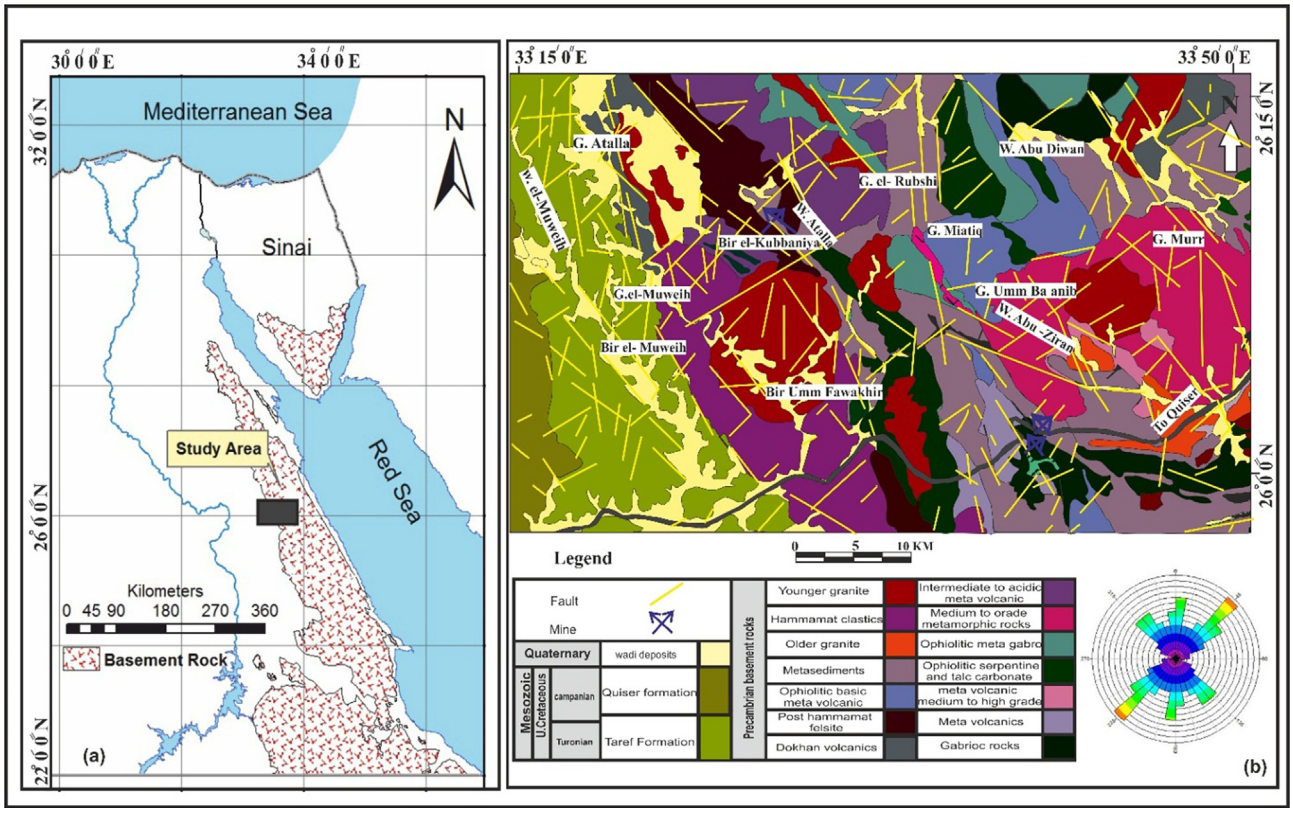

Fig. 1. a – Location map of the study area, b – Geological map of the study area modified after Conoco, 1987.

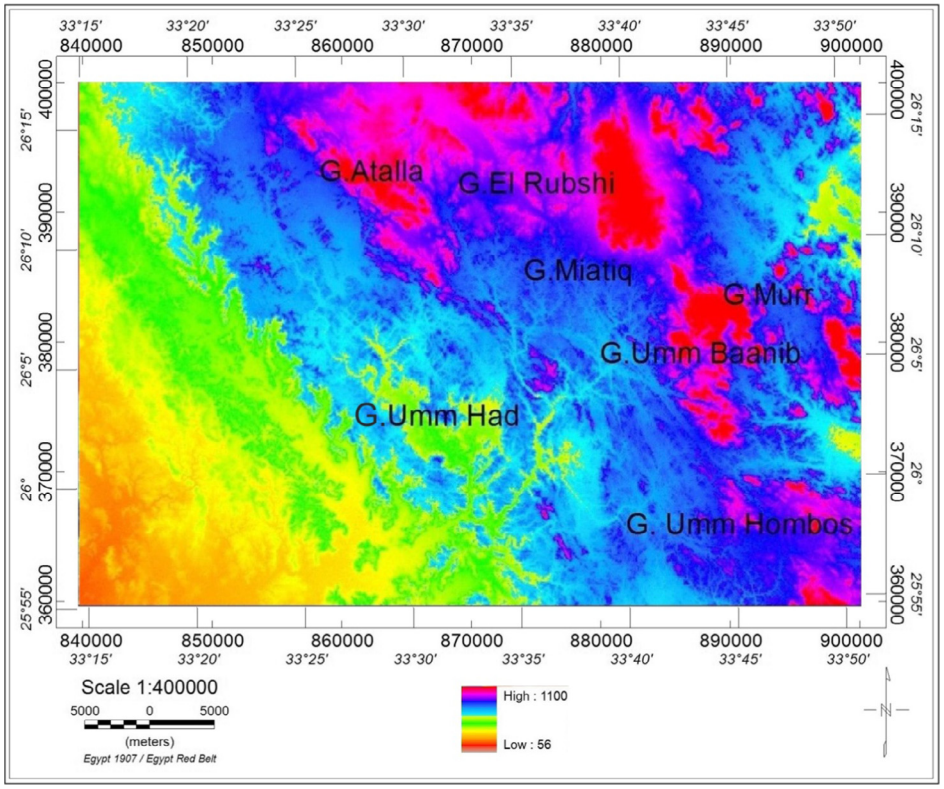

Fig. 2. SRTM DEM of the study area showing the topographic variation.

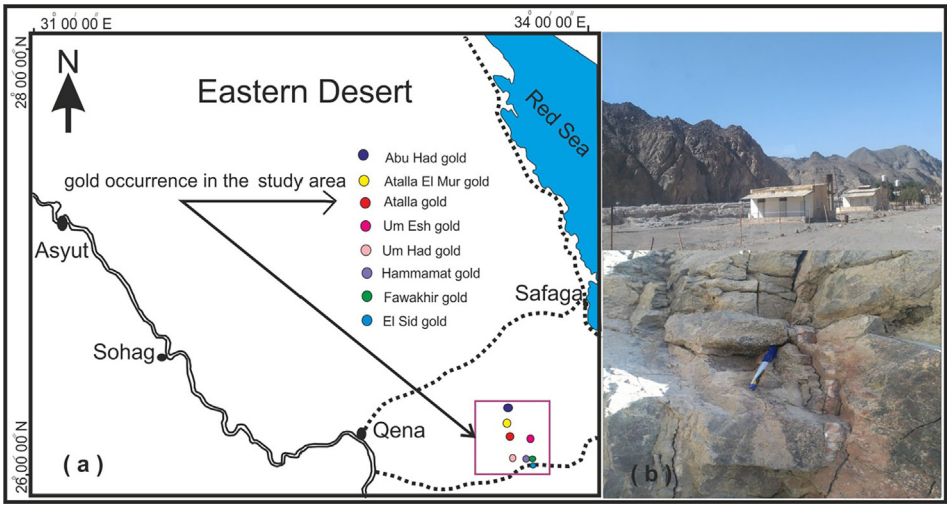

Fig. 3. a – Gold occurrences in the study area modified from the Egyptian geological survey and Mining Authority map 1994, b – Field photos around mine areas.

(EGSMA). The survey was implemented following parallel flight lines in the NE-SW direction at 1.5 km space interval with an azimuth of 45° and 225° from the true north. A high-sensitivity256-channel airborne gamma ray spectrometer was used to carry out the gamma ray spectrometric survey. The data of the survey was available in the form of total magnetic intensity, total count, Potassium, equivalent Uranium, and equivalent Thorium contour maps, which were digitized to obtain a digital form of the survey data for enhancement and interpretation processes done by using Oasis Montaj software.

4. Processing operations

4.1. Aeromagnetic data

To assist delineation of lineaments and create structural complexity maps, firstly, the total magnetic intensity map (Fig. 4) was reduced to the pole to locate the magnetic anomalies above their source bodies. thereafter, several enhancement procedures were carried out on the resulted RTP map (Fig. 5) to clear the picture for interpretation as follow:

4.1.1. Vertical and total gradient

First vertical derivative can be applied either in space or frequency domain. It is proposed by Nabighian (1984), using 3D Hilbert

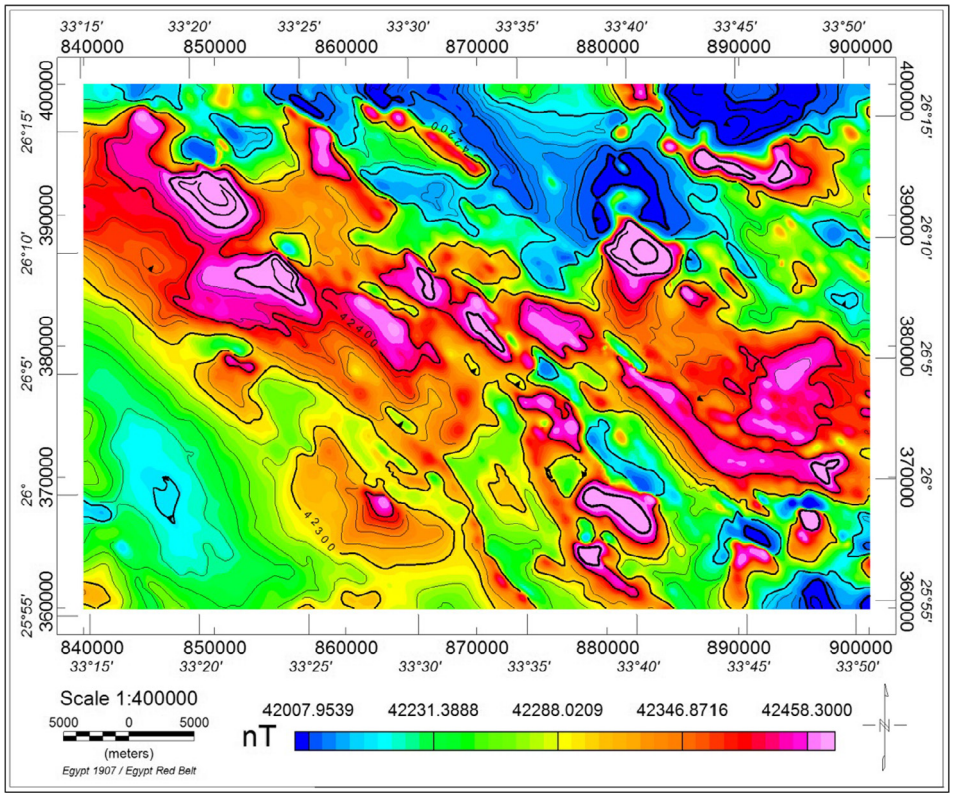

Fig. 4. Total magnetic intensity map of the study area.

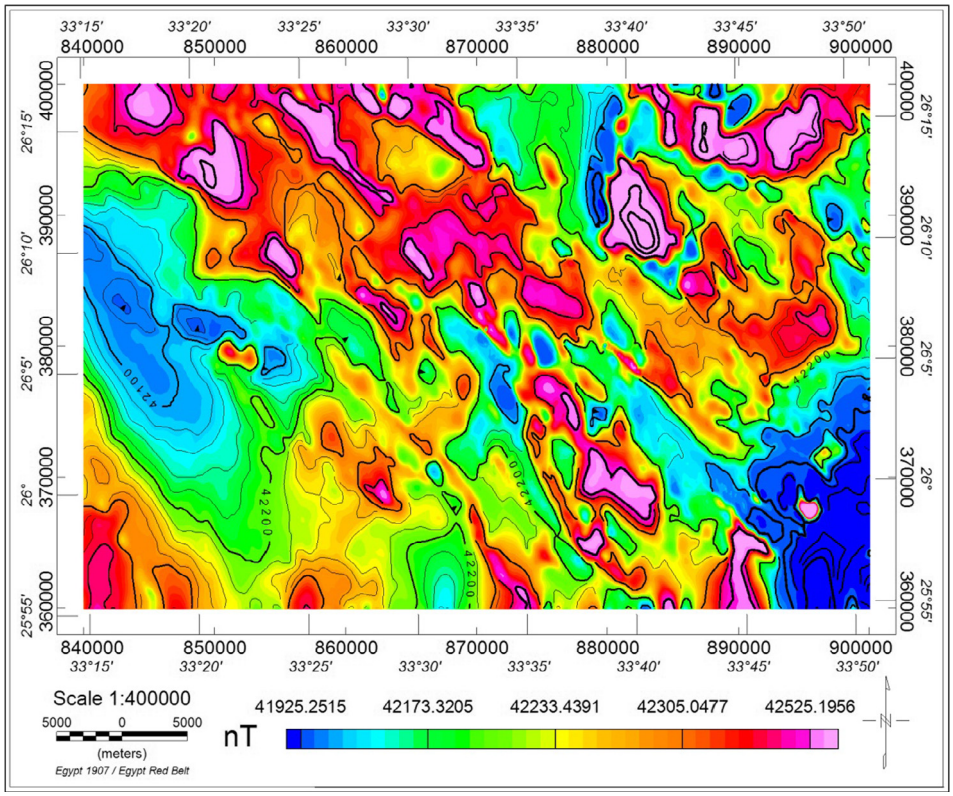

Fig. 5. Reduction to pole map of the study area.

transforms in the x and y directions. It is used in this study to enhance shallow features with their boundaries and associated lineaments. It amplifies short-wavelengths at the expense of longer ones. So, shallower causative sources can be outlined and mapped. Also, the analytic signal (total gradient) can be calculated either in space or frequency domain, generating a maximum directly over discrete bodies as well as their edges. It is formed through the combination of the horizontal and vertical gradients of the magnetic anomaly (Ansari and Alamdar, 2009) and its amplitude is independent on the magnetisation direction. This filter applied to reveal the anomaly texture and highlight discontinuities also enhance short- wavelength anomalies (Roest et al. 1992).

4.4.1.2. Centre for exploration targeting grid analysis. Centre for Exploration Targeting (CET) is a suite of algorithms which provides functionalities for enhancement, lineament detection and structural complexity analysis of potential field data (Holden et al. 2008; Core et al. 2009). This technique automatically delineate lineaments and identify promising areas of ore deposits via outlining regions of convergence and also divergence of structural elements using several statistical steps that include texture analysis, lineation delineation and Vectorisation and complexity analysis to generate contact occurrence density map.

4.1.3. Centre for exploration targeting porphyry analysis

Porphyry – like intrusions are circular or semi-circular features with their rims or boundaries being zones of weakness that help to ascend hydrothermal solutions. To locate these features and hydrothermal alteration associated with them the CET porphyry approach was applied to the RTP data of the studied area. The intrusion itself and the alteration zone are usually associated with positive magnetic anomalies whilst the outer alteration zones are much less magnetic (Macnae, 1995). The approach was conducted firstly, by using steps on circular feature transform and the central peak detection techniques. Then applying Amplitude contrast transform, the boundaries or rim of the sources were defined. Finally, the whole configuration was depicted through tracing.

4.2. Aeroradiometric data

The aeroradiometric technique assists considerably in mapping surface structure, lithological units and identification of hydrothermal alteration zones. The radiometric data are gridded to obtain total count, potassium, equivalent thorium and equivalent uranium maps to show the surface distribution of these elements and delineate surface lineaments. Also, producing K/eTh ratio map help to map hydrothermally altered zones, since a reduction in eTh and a rise in K is an indicator of alteration environments in an ore deposit (Ostrovskiy, 1975). Finally, A ternary map is created by combining the three radioelements concentration in the RGB colours.

5. Results and discussions

In the present work, aeromagnetic and aeroradiometric data of a part of the Central Eastern Desert of Egypt were enhanced and analyzed for subsequent interpretation, by applying a number of selected filter. The resulted map forms of these steps include the following:

5.1. Derivative maps and geologic structures

The vertical derivative map (Fig. 6) gives a good representation of near surface features such as faults (green and blue lines) where the filter enhances short-wavelength anomalies responsible for shallow sources at the expense of long ones. It is outstanding to note that the eastern part of the study area was occupied by such short-wavelength anomalies indicating a relatively shallow depth of the causative sources in comparison with the western part where we can be concluded a more deeper sources conformable with the presence of a sedimentary cover.

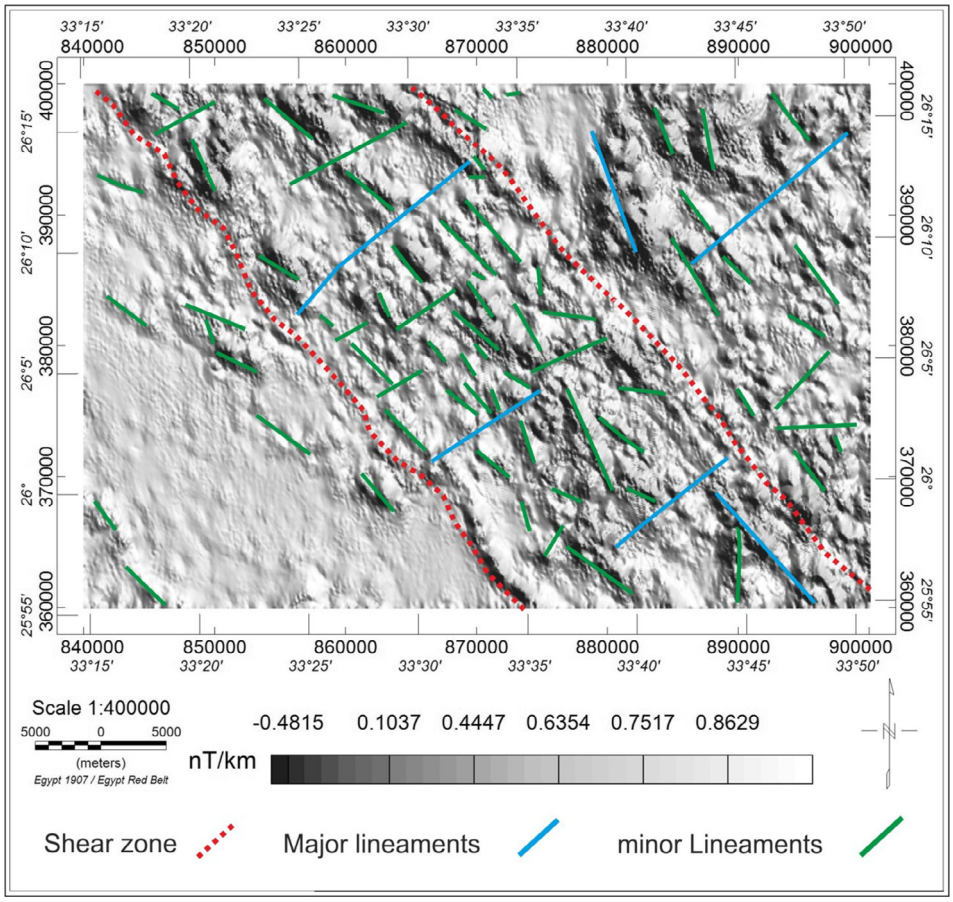

Fig. 6. First vertical derivative map of magnetic data in gray scale with mapped structures.

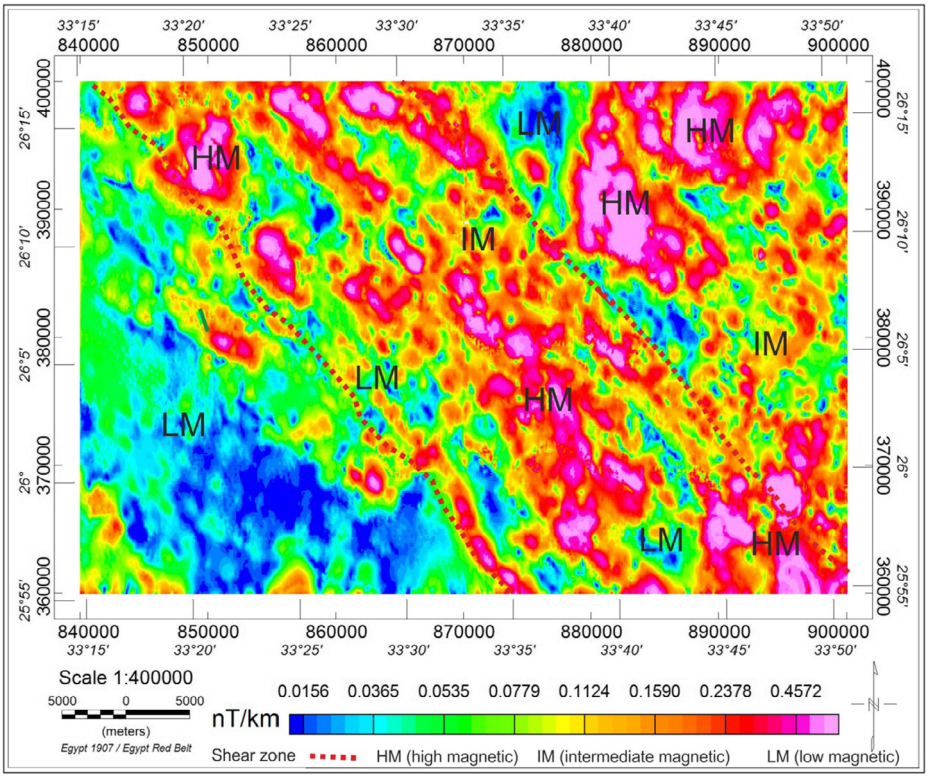

Fig. 7. Analytical signal map of the RTP data.

A glance at the map clears that the NW trend is the most pronounced directions in the area and the associated NE-SW, E-W and N-S directions come in the following orders respectively.

The analytical signal map (Fig. 7) accentuate the variation in the magnetization of the magnetic sources in the study area and highlights discontinuities and anomaly texture. On comparison with FVD (Fig. 6) the differentiated and undifferentiated complexes have been redefined and properly mapped not only based on their depths but mineralogical compositions as well. As a result, the high magnetic anomalies zones are associated with highly rich ferromagnesian-bearing rocks with minor felsic minerals (Telford et al., 1990). Therefore, AS map exhibited three different magnetic zones. Low to fairly low magnetic zone (LM) with a gradient 0.0156–0.0779 nT/km associated with clastic sediments, hammamat clastics, metavolcanic, metasediments, and granite because these rocks contain more than 60% quartz. The moderate zone (MM) with gradient 0.0779–0.2378 nT/km associated with granite – gneiss as these rocks contain high ferromagnesian with low amount of felsic minerals. The high magnetic anomalies zones (HM) 0.2378–0.4572 nT/km are related to ophiolitic serpentine, ophiolitic metagabbro, gabbroic rocks, dokhan volcanic and hammamat felsite as these rocks have high ferromagnesian with large amount of felsic minerals.

Additionally, these anomalies seems to be structurally controlled by the observed trends in the NW-SE and NE-SW direction with minor traces of the E-W and N-S ones.

The shear zones are not clearly observed on the geologic map (Fig. 1b). meanwhile it is very well pronounced on the FVD (Fig. 6) and AS (Fig. 7) maps, where a distinctive belt with very small closed anomalies aligned nearly NW- SE direction is observed in both maps. Contacts trending in NW and NNW directions from both sides mainly bound this belt on the geologic map. They have the appearance of structural contacts on the FVD and AS maps where faults occupying their locations follow the peaks of small closed anomalies.

5.2. CET grid analysis

The approach was carried out to identify linear structures contained within the aeromagnetic data via consecutive map byproduct forms that include standard deviation which estimates magnetic variations, then phase symmetry to separate laterally continuous lines. Thereafter, the resulted lineaments enhanced by suppressing noise and background signals using an amplitude thresholding Fig. 8.

It is worth mentioning that the lineaments exhibited by the Vectorisation map (Fig. 8) reveal the basement rocks that occupy the eastern part of the area are highly deformed as compared with the western part covered by cretaceous sandstone. It is also evident in the accompanied rose diagram that The NW-SE, NNE-SSW and NNW-SSE trends are the most prominent ones with minor traces of NE-SW direction.

The analysis of aeromagnetic maps lead to delineate a geological and structural map Fig. 9. A large number of faults and shear zone have been identified using the various filtered techniques particularly the FVD, AS and Vectorization.

Complement to that the contact occurrence density heat map (Fig. 10), which is based on the automated lineament detection output and the traced ones from FVD and AS displays the relationship between the expected complexity structural zones and known gold mineralization obtained from the metallogenic map for Egypt in the study area. Clearly, these areas correspond to a series of deposits that have preferred Northwest- Southeast directions.

5.3. CET porphyry analysis

In the present study, detection of porphyry features was conducted in four successive steps including at first circular feature detection. Secondly, Amplitude contrast transform then Boundary tracing which overlaid on the RTP map of the study area in Fig. 11. Finally, an occurrence density map that depicts porphyry features was generated Fig. 12. Most of these dike-like features are more abundant above

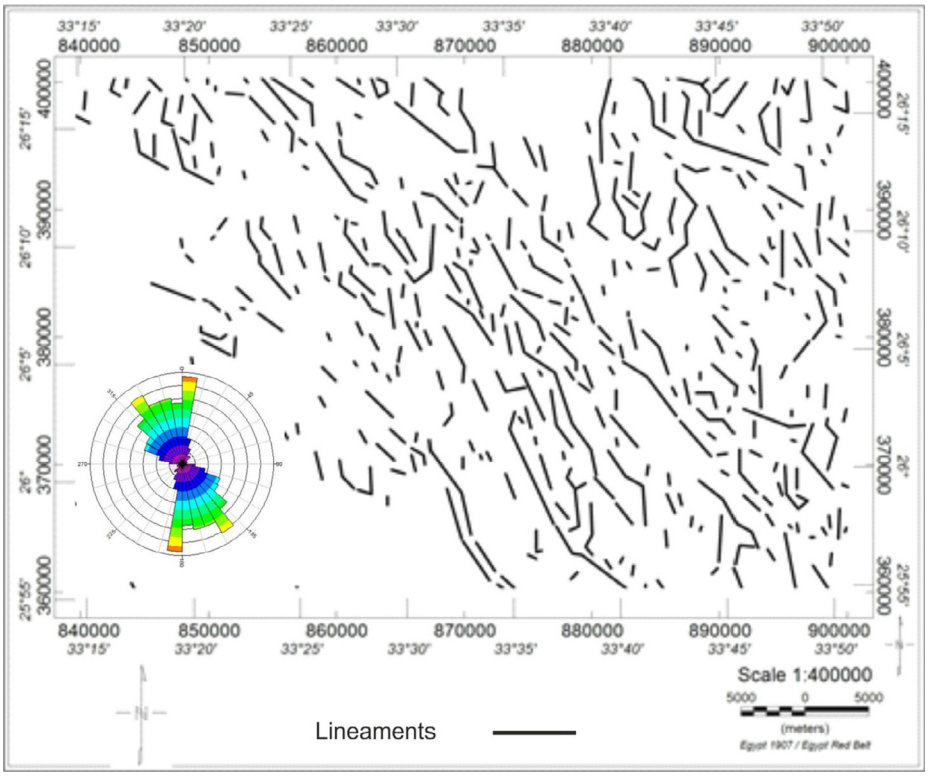

Fig. 8. Vectorisation lineaments map.

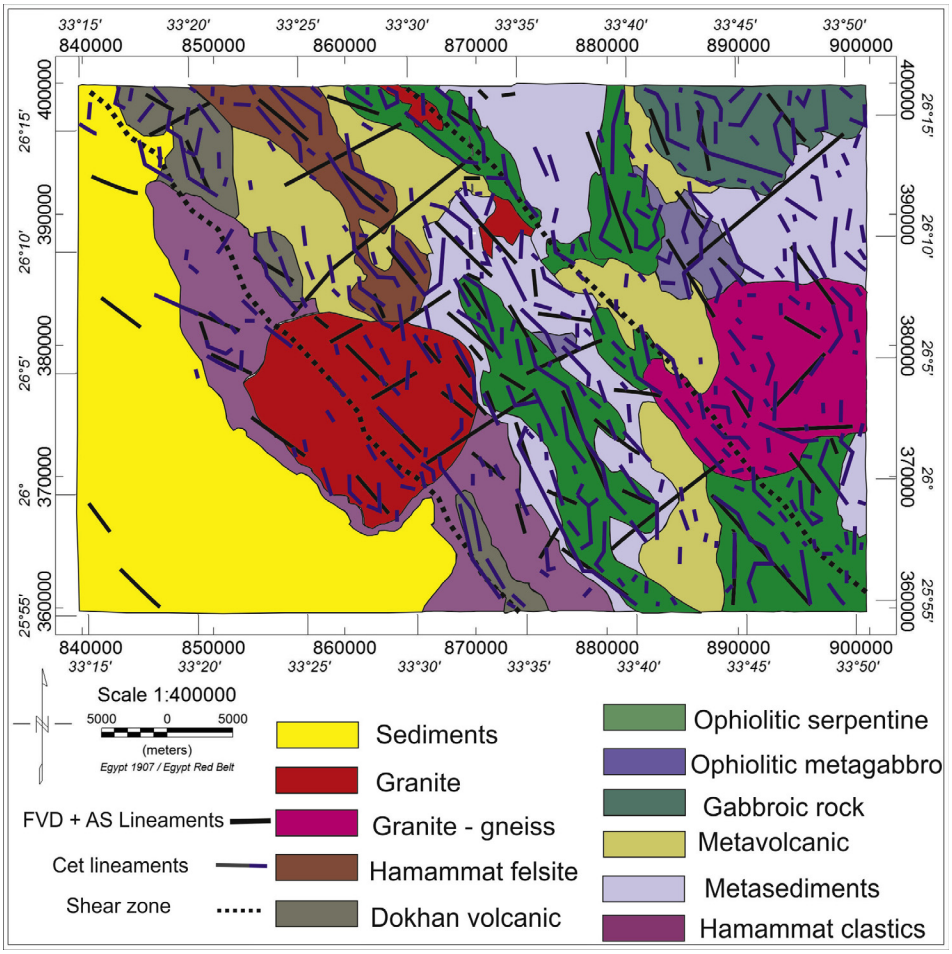

Fig. 9. Proposed structural and geological map delineated from aeromagnetic data.

granite, serpentine, metavolcanics and Dokhan volcanic. It was observed that these features are in coincidence with the structural complexity heat maps obtained from both of CET grid and porphyry analysis. It is also worth noting that these features are located along the NW-SE trend which represents the preferred orientation for ore deposition and indicating a high probability for further ore deposition in the study area. Meanwhile, the known mineralization areas were also plotted on the same map and it was found that the mineral occurrences, in most cases are above these porphyry features or close to.

The evident agreement between the density maps (Figs. 10 and 12) and the good matching of the known mineralizations sites in the study area with the interpreted structures and porphyry forms allowed predicting and mapping new areas of high probable mineral resources, these are South G. Mi'tiq, Northeast G. Umm Ba'anib, East w. Abu Diwan, around Bir El-Kubania and West W. Atalla and needs only fellow up in the field to determine its full potential. Furthermore, these information will be more valuable when integrated with radiometric data sets that were used in the detection of hydrothermally altered mineralization zones.

5.4. TC, K, eTh and eU concentration maps

In the total count contour map (Fig. 13) the lowest concentration level ranges from (6 to 16 μR/h) is associated with Metavolcanics (mv), Ophiolitic Metagabbro (mgo), Ophiolitic Serpentine and Talc Carbonate (sp) around G. Mitiq, G. El-Rubshi and W. Abu-Diwan. The moderate concentration level ranges from (26 to 65 μR/h) is observed at the western and central part of the study area and related to Quseir (kuq) Taref formations (kut) around W. el Muweih, W. el Atwani, G. El Gir and Hammamat Clastics (ha) in the south-eastern of the study area. The high level concentration that ranges from (65 to 92 μR/h) is associated with Younger granite (g_β), Metamorphic rocks (gnl), Dokhan volcanic, Post Hammamat felsites (vf) around G. Attala, G. Umm Had, G. Murr and G. Umm Ba'anib.

The K contour map (Fig. 14) shows that Metavolcanics (mv), Metagabbro (mgo), Ophiolitic Serpentine and Talc Carbonate rocks (sp) have lowest concentration level (1–3%). While, the metasediments (ms), Taref (kut) and Quseir formation (kuq) have the moderately level (3–18%); Dokhan Volcanic (vd), Post Hammamat Felsites (vf), Metamorphic rocks (gnl) and Younger granite (g_β) have the highest one (18–27%).

The lowest concentration level in the eTh contour map (Fig. 15) are related to Metavolcanics (mv), Metagabbro (mgo), Ophiolitic Serpentine and Talc Carbonate rocks (sp). The highest level reaches to 91 ppm is associated with younger granite (g_β) while, Dokhan Volcanic (vd), Post Hammamat Felsites (vf) and Taref formation (kut) have the moderately level.

The eU map (Fig. 16) indicates that the high level of uranium concentration is associated with the younger granite (g_β) and metamorphic rocks (gnl). while, Metavolcanics (mv), Metagabro (mgo), Ophiolitic Serpentine and Talc Carbonates rocks (sp) have the lowest one. The moderate level is associated with Metasediments (ms), Hammamat Clastics (ha) and Post Hammamat Felsites (vf), Quseir (kuq) and Taref formation (kut).

It was clear that there is a near agreement between the indicated levels of radioactivity and the corresponding rock types. The major linear trend, which could be interpreted from the elongation of the radiometric anomalies is NW-SE trend. Accordingly, the NW-SE trend

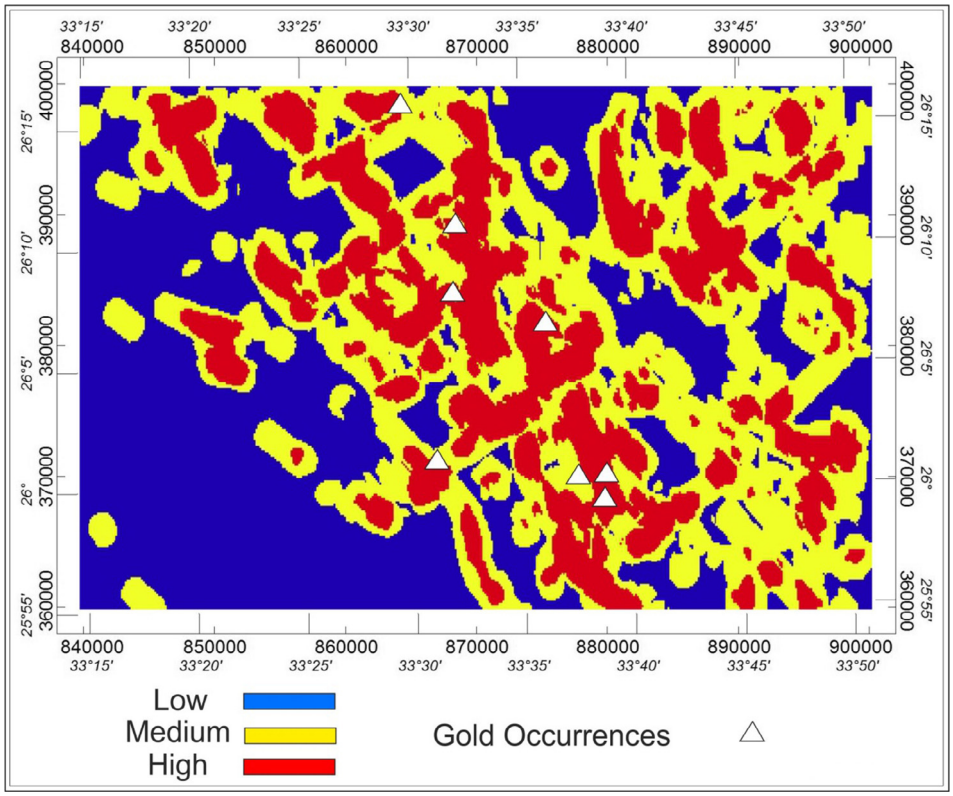

Fig. 10. Density map of aeromagnetic Lineaments overlain by known gold occurrences.

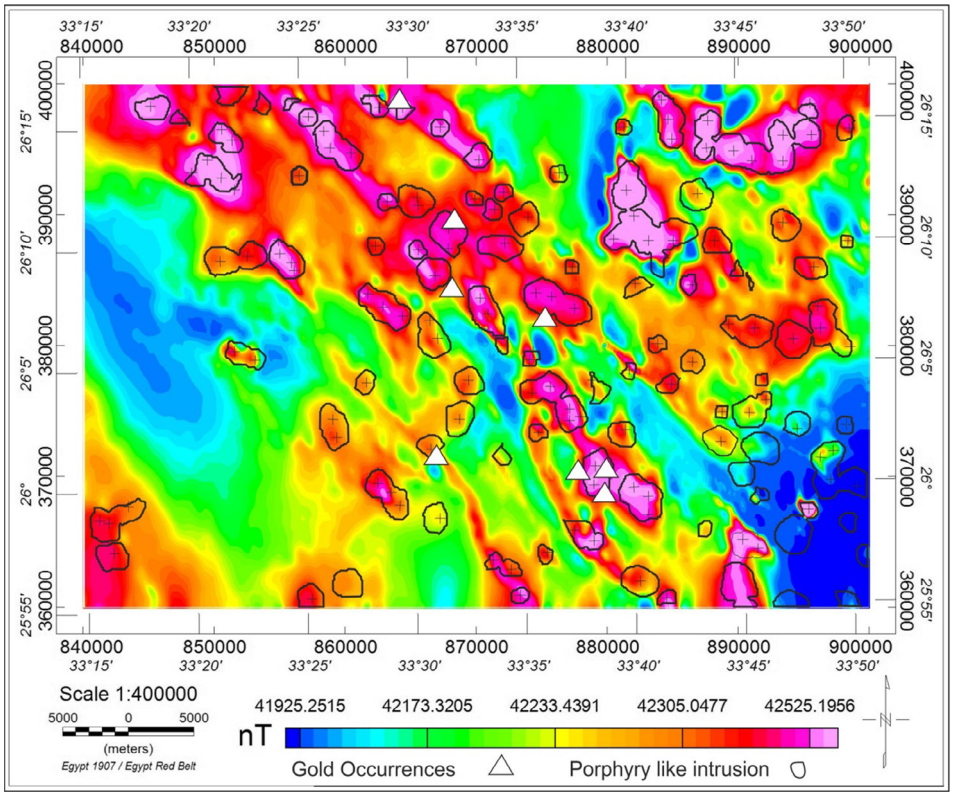

Fig. 11. Boundary tracing on the RTP map of the study area overlain by known gold occurrences.

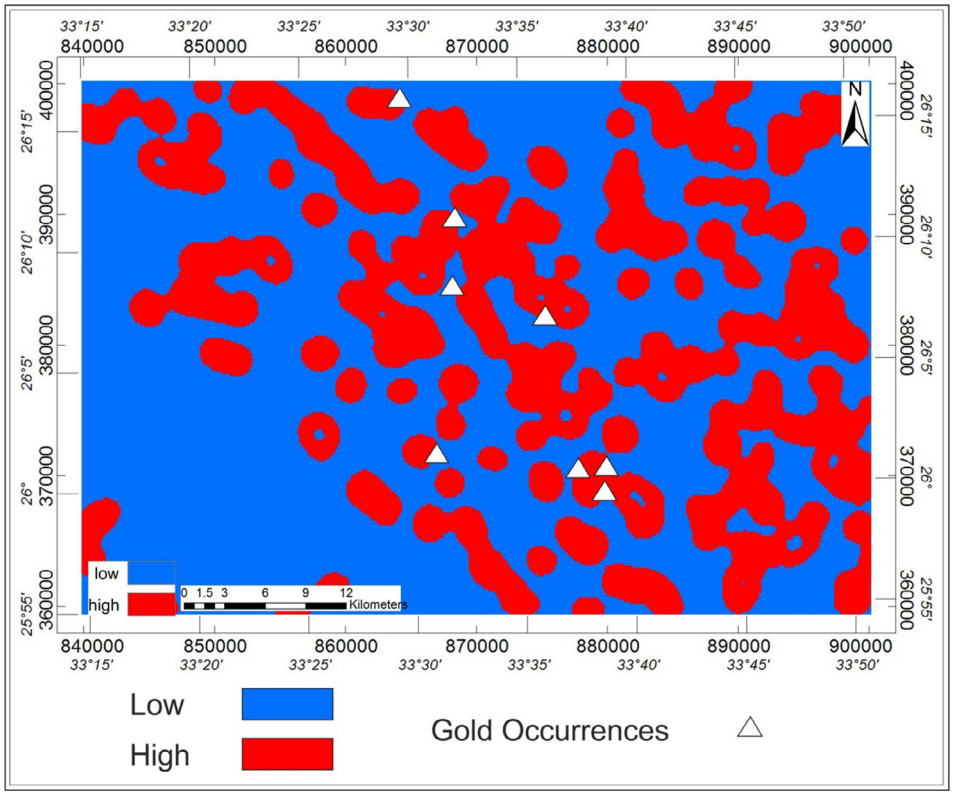

Fig. 12. Density map of the porphyry intrusion overlain by known gold occurrences.

seems to be the most identified trend from both aeromagnetic and aeroradiometric interpretation, and that confirms the effective role of this trend on in the geological frame of the study area. Some other trends (NE-SW, E-W and N-S) could be traced from other elongated bodies of the radiometric anomalies.

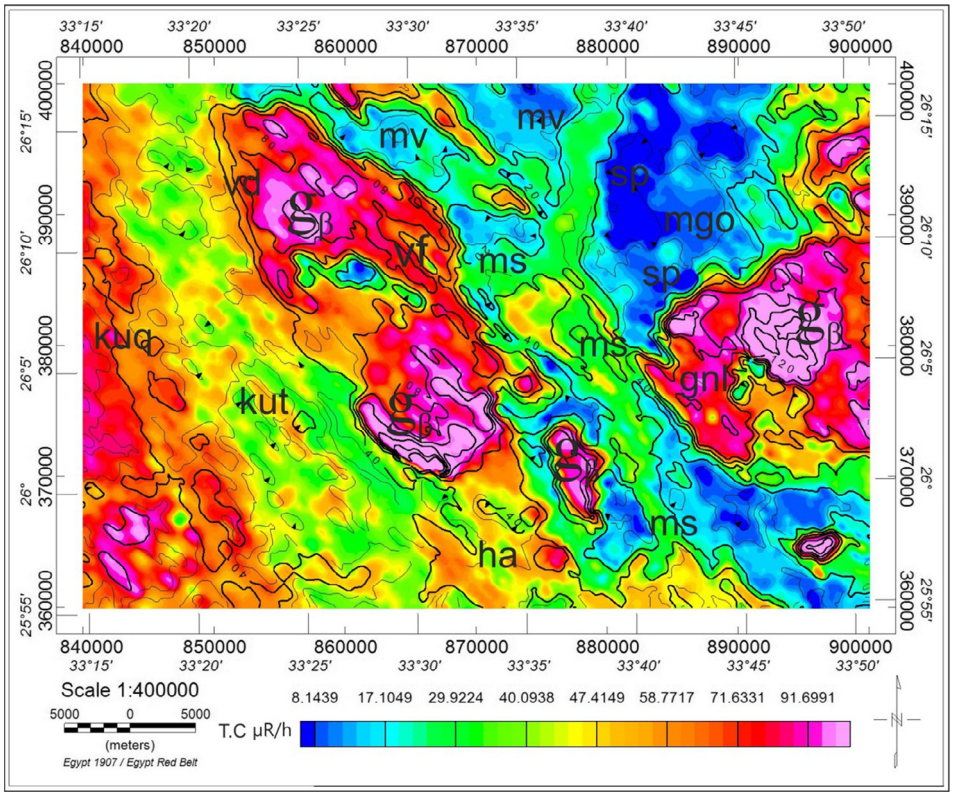

Fig. 13. Total count map.

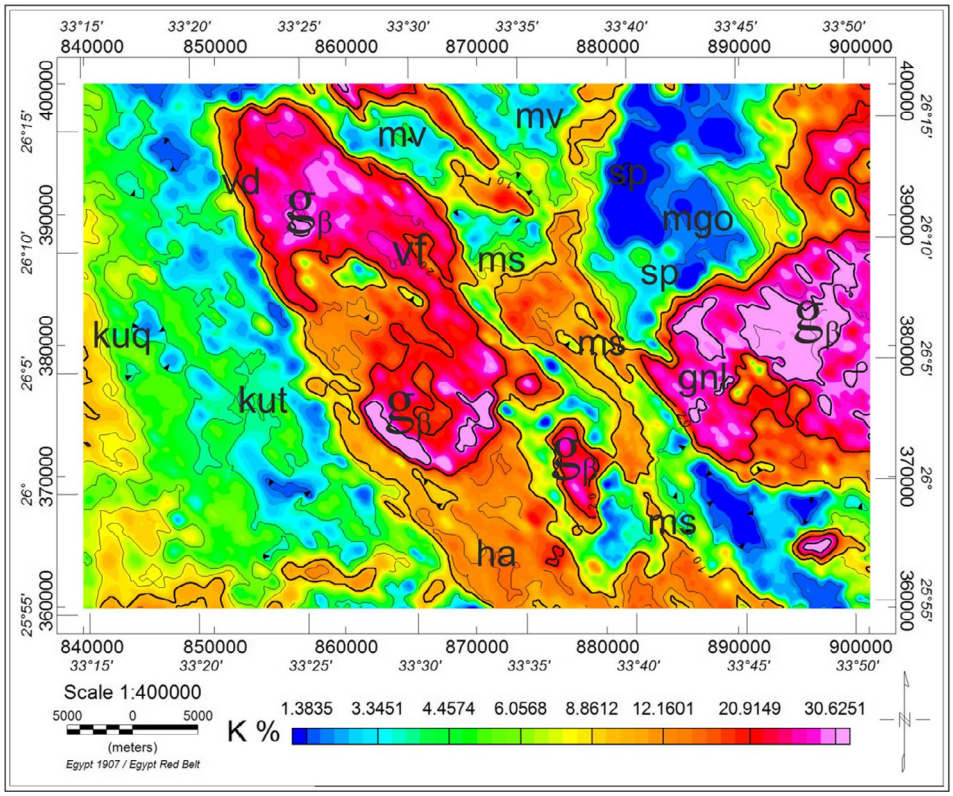

Fig. 14. Potassium (K) concentration map.

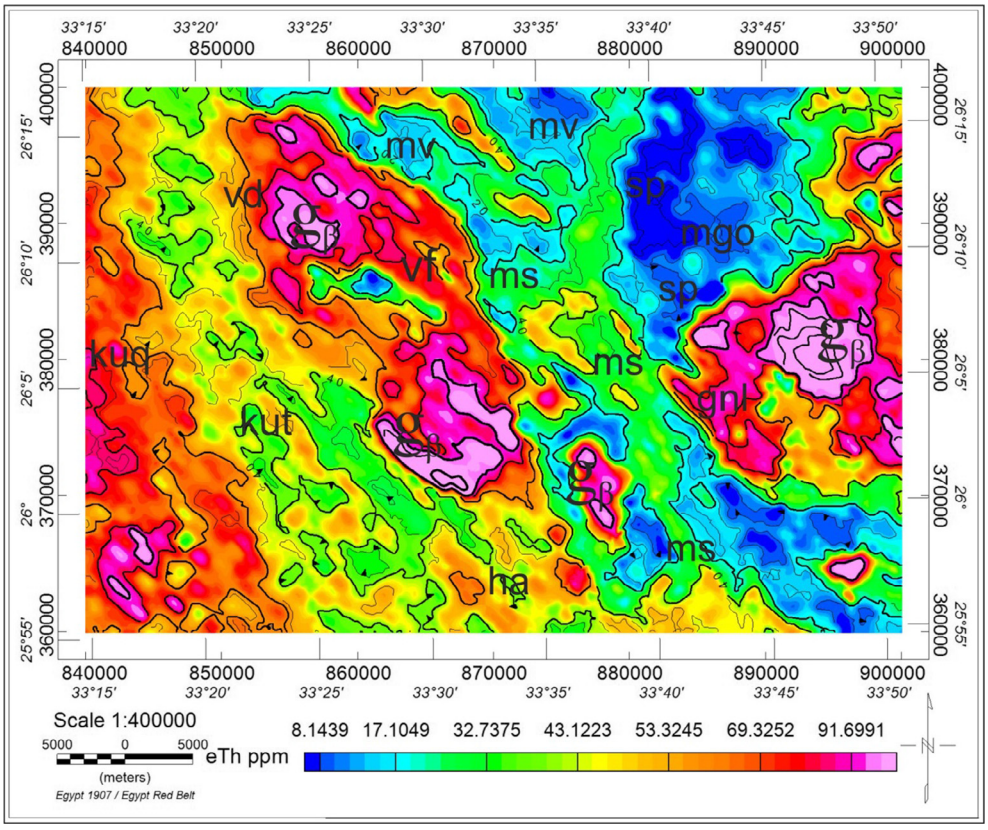

Fig. 15. Equivalent Thorium (eTh) concentration map.

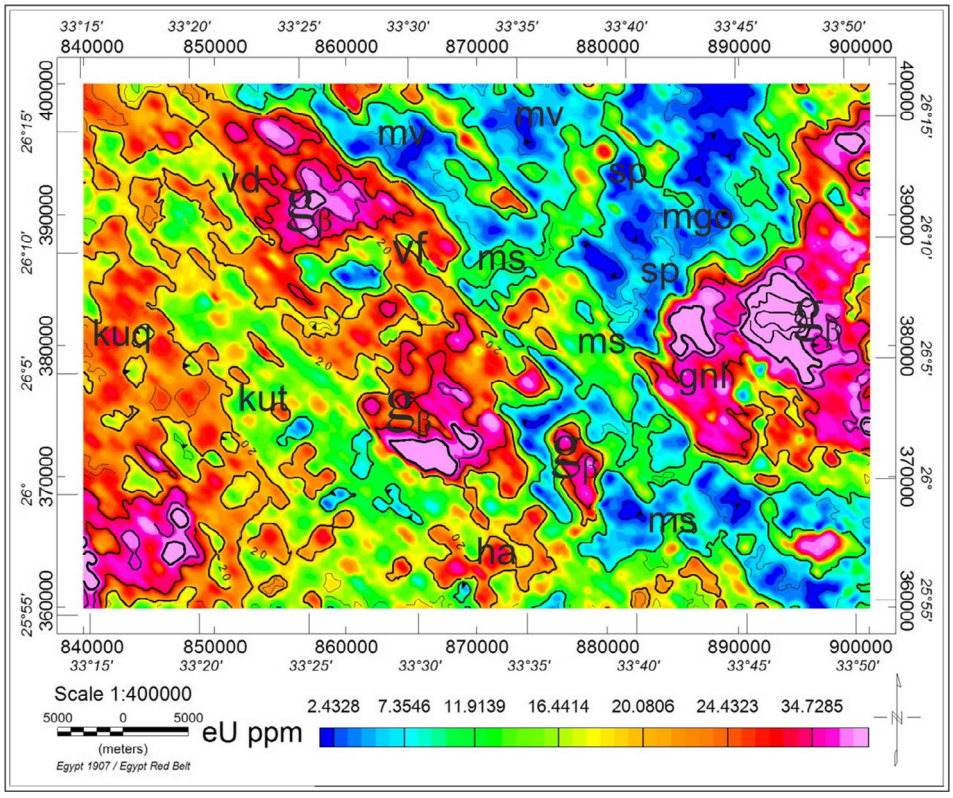

Fig. 16. Equivalent Uranium (eU) concentration map.

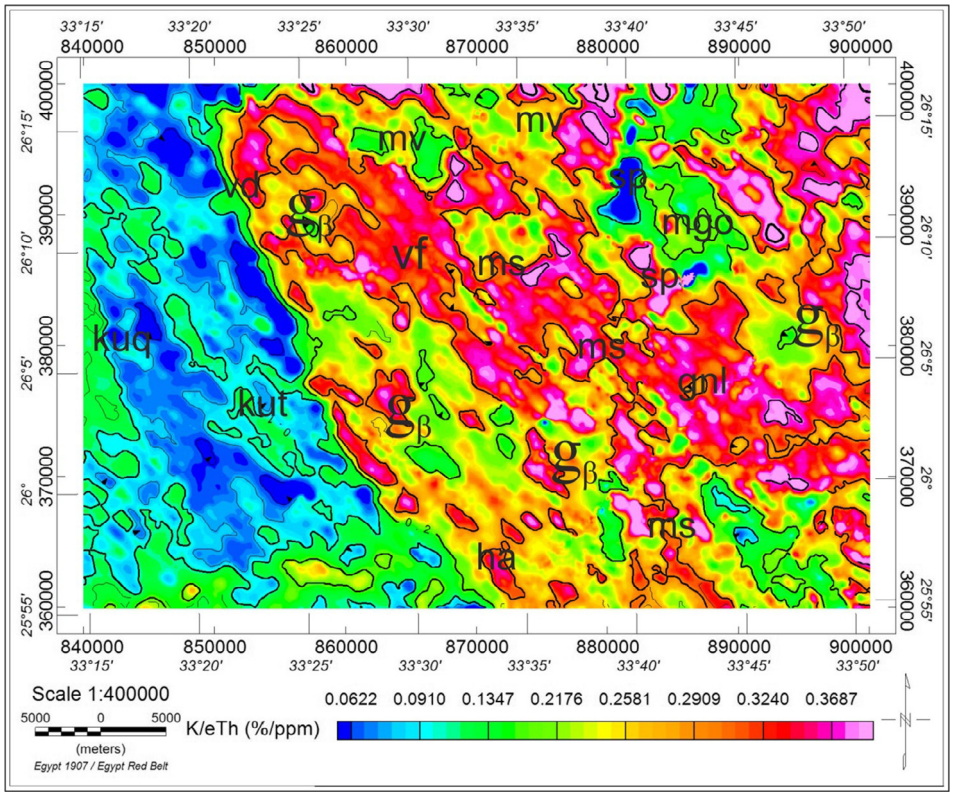

Fig. 17. Potassium Thorium (K/eTh) ratio map.

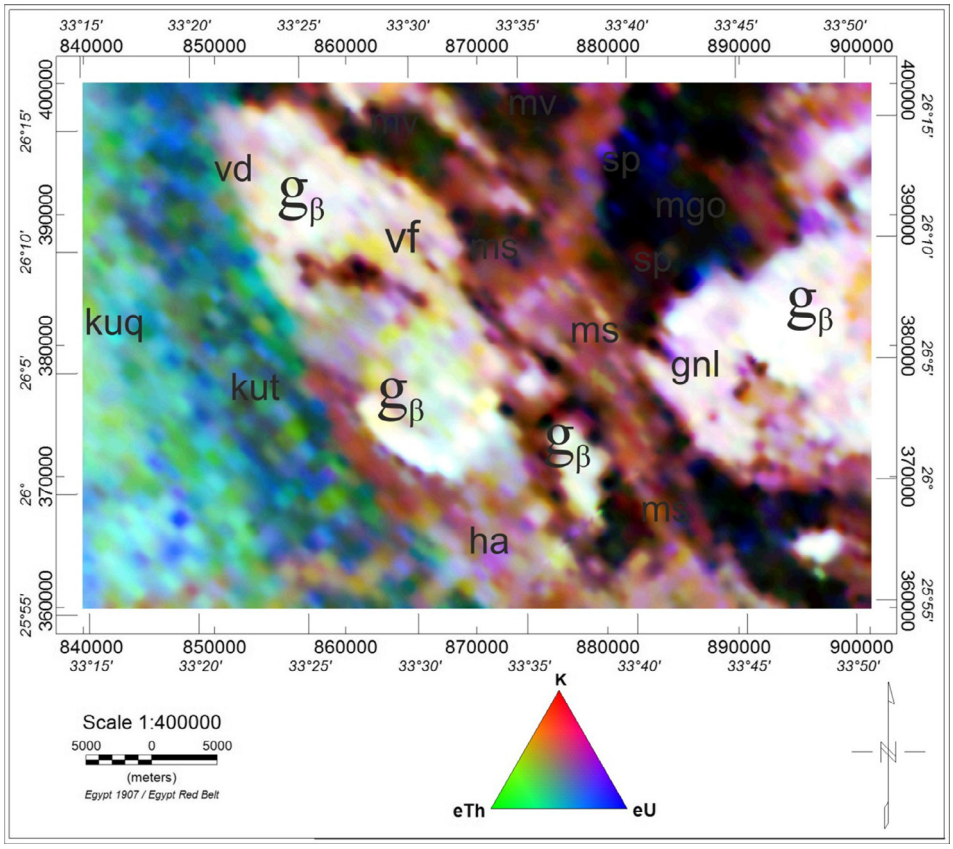

Fig. 18. Radiometric ternary map.

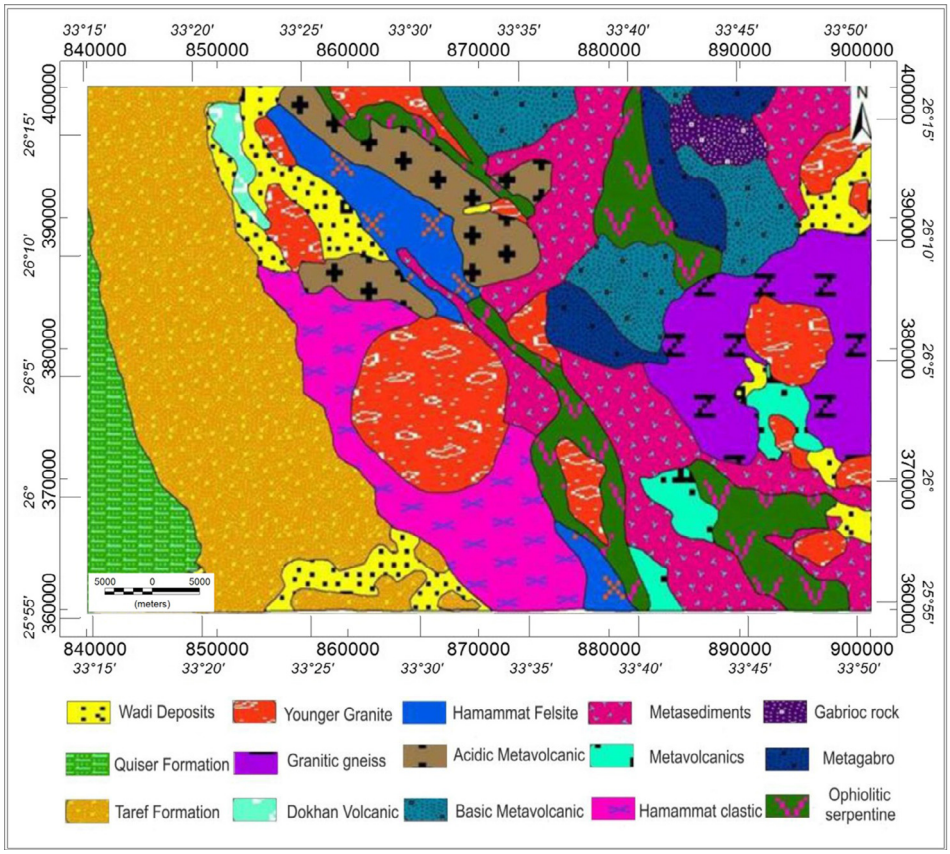

Fig. 19. Lithological map interpreted from radiometric data.

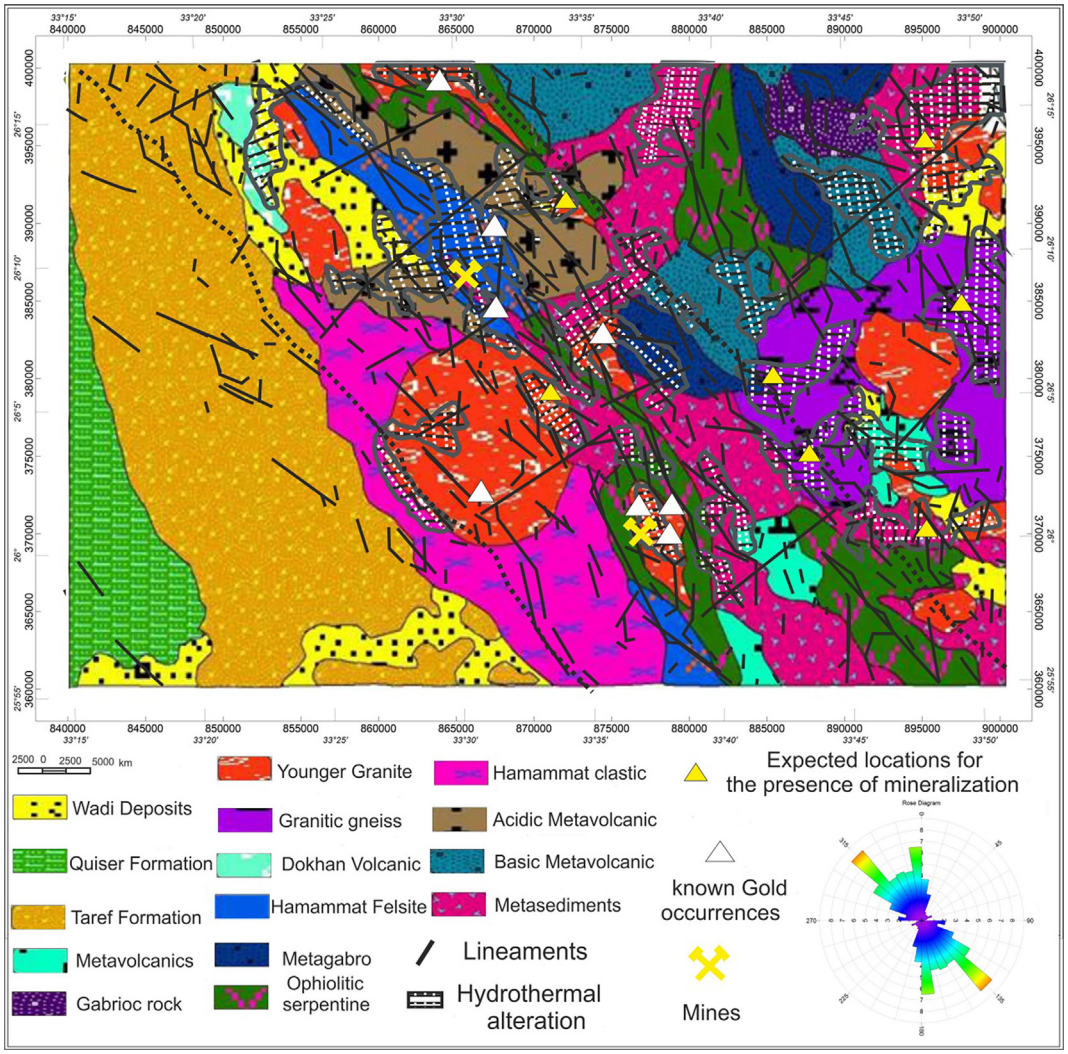

Fig. 20. A composite map of aeromagnetic, aeroradiometric and Geologic data.

5.5. K/eTh ratio map

As potassium is more mobile than thorium, K/eTh ratio anomalies can be distinguished to areas of hydrothermal alteration which are characterized by K enrichment. However, depending on the fact that the ratio between potassium and thorium is rather constant in most rocks, typically varying from 0.17 to 0.2 (K/Th in%/ppm, Hoover et al. 1992). Rocks with K/eTh ratios remarkably outside of this range have been named potassium or thorium specialized (Portnov, 1987). So, the zones characterized by the high K/eTh ratio values are the strong indicator of hydrothermal alteration. From the K/eTh ratio map (Fig. 17) it is seen that the areas affected by the hydrothermal process is featured by pink color and have a high value about 0.3687 of K/eTh ratio. These areas associated with younger granite, Hammamat felsites and Metasediments in the eastern part of the study area. Also, the map clearly showed that the interpreted alteration zones were following the NW-SE trend which was deduced as the major trend in the studied area.

5.6. Ternary and interpreted lithological maps

The ternary map (Fig. 18) of the study area was established by modulating the three colors blue, green and red for the intensities of Potassium, thorium and uranium respectively. The radiometric response in the ternary map to some extent corresponds with the surface rock units of the study area and shows a close spatial correlation with the rock units. The visual inspection of this map shows that high concentration of K, eTh and eU radioactive elements are displayed in white color and related to Younger Granite (g_β), Metamorphic rocks (gnl), Dokhan Volcanic (vd) and Post Hammamat Felsites (vf). They are normally characterized by their strong radiometric response and can be easily discriminated from the low radioactive rocks. Low concentration of K, eTh, and eU radioactive elements is represented by dark color coincides with Metavolcanics (mv), Ophiolitic Metagabro (mgo), Ophiolitic Serpentine and Talc Carbonate rocks (sp). The blue color represents high potassium content but low thorium and uranium and coincides with Hammamat Clastics (ha) and Metasediments (ms). Additionally, the green color corresponds to regions of high thorium with low potassium and uranium associated with Taref Formation (kut). The composite image does not provide color discrimination between Metavolcanics, Metagabro, Ophiolitic Serpentine and Talc Carbonates rocks (sp) also there is no color discrimination between Metasediments (ms) and Hammamat clastics (ha). This can be discussed to the resemblance of radioelement content and the redistribution of radioelements concentration in the overburden because of high weathering process.

The total count map together with the ternary image was used to construct an interpretative radiometric lithological map (Fig. 19). Carefully inspection of this map and its rapprochement with the geological map presented by Conoco (1987) (Fig. 1b) highlights some conspicuous features. They obviously expose the basement and

sedimentary contacts. Most of the traced rock units of the basement complex such as Younger granite, metamorphic rock, Dokhan volcanic, metasediments, acidic and basic Metavolcanics, Gabbro, ophiolitic serpentine, talc carbonates and Metagabro are in close agreement with the rock units presented in the geological map.

6. Data integration

The results of aeromagnetic, aeroradiometric data sets and geology were integrated to produce a composite map of the study area (Fig. 20). A critical inspection of this map showed that the eastern part of the study area is highly faulted compare to the western part. The predominant tectonic trends are NW, NNW, NNE, WNW, NE, E-W and N-S. The NW-SE (Gulf of Suez or Red Sea trend) was the most developed one among these trends and represents the preferred orientation of ore deposits. Also, a number of hydrothermally altered zones are mapped from the K/eTh ratio map (Fig. 9). Since these zones have one or more structures associations, they serve as channel pathways for migrating hydrothermal fluids that contemporaneously reacts with rock formation which got altered subsequently. The alteration zones marked by low magnetic intensity and high potassium content that lie within or close to a structure that has a NW trend identified previously. The concidence areas of these alteration zones and high complexity lineaments and porphyry indicated a high possibility for the occurrence of gold mineralization in other similar locations. The known area of gold mineralization (Abu Had, Atalla, Atalla El Mur, Um Esh, Um Had, Hammamat, Fawakhir and El Sid gold) were overlain in the map with white triangles shapes where most of these locations are structurally controlled by NW-SE directions and lain on hydrothermally altered zone which represent good features for gold occurrence. Thus, as mentioned previously the tight concordance between these known mineralization locations and the interpreted structural complexities sheds a light towards the similar mapped features that may be new promising sites. These probable locations were marked by yellow triangles shapes. However, precise detection and evaluation of these ores need more geological and geophysical follow up survey with finer spacing.

7. Conclusion

Interpretation of the available aeromagnetic and aeroradiometric data sets besides the other constructed maps revealed that the NW trend is the most prominent one with some minor trends aligned in NW, NNW, NNE, WNW, NE, E-W and N-S directions. The CET Grid analysis and Porphyry show a close conformity between our estimated structural complexity, porphyry (dike-like) and known mineralization areas observed on the metallogenic map of Egypt in the study area. Clearly, these areas are characterized by an increased feature intersection density as well as feature orientation diversity. Based on these evidence other areas have similar criteria are observed and may represent a strong indicator for the occurrence of ore deposits such as South G. Mi'tiq, Northeast G. Umm Ba'anib, East W. Abu Diwan, around Bir El-Kubania and West W. Atalla. The aeroradiometric maps assisted in correlating the distribution of the radioactivity elements with the rock units, mapping of lithology and hydrothermal alteration zones. The high value of K/eTh ratio map gives a strong indicator for mapping hydrothermal alteration zones. The Metasediments, Hammamat felsites, metamorphic complex (Um Ba'anib granite gneiss) granite rocks are seen to be structurally altered more than others. Ternary map with total count map used to remapping lithological units based on the variety on the concentration of radioelements and ratio. These results were combined to produce a composite map of the study area consisting of the geology, structures, hydrothermally altered zones and the areas of promising mineralization.

References

Akawy, A., 2009. Structural elements and incremental strain history of the basement rocks of Um Had area, central Eastern Desert, Egypt. Arab. J. Geosci. (Print) 2 (4), 285–300.

Ansari, A.H., Alamdar, K., 2009. Reduction to the pole of magnetic anomalies using analytic signal. World Appl. Sci. J. 7, 405–409.

Andrson, H., Nash, C., 1997. Integrated lithostructural mapping of the Rossing area, Namibia, using high-resolution aeromagnetic, aeroradiometric, Landsat data and aerial photographs. Explor. Geophys. 28, 185–191.

Aero Service, 1984. Final report on airborne magnetic/radiation survey in Eastern Desert, Egypt. Work Completed for the Egyptian General Petroleum Corporation (EGPC). Six volumes, Aero Service, Houston, Texas, USA.

Abd El Nabi, S.H., 2013. Role of γ-ray spectrometry in detecting potassic alteration associated with Um Ba'anib granitic gneiss and metasediments, G. Meatiq area, Central Eastern Desert, Egypt. Arab. J. Geosci. 6, 1249–1261.

Abd El Rahim, S.H., El Nashar, E.R., Osman, A.F., Abd El Ghaffar, N.I., 2013. Gold-bearing sulphides associated with the granitic wall rock alterations at the Fawakhir area, Central Eastern Desert, Egypt. In: 7th European Conference on Mineralogy and Spectroscopy, ECMS.

Abu-Alam, T., Grosch, E., El Monsef, M.A., 2013. Pan-African shear zone-hosted gold mineralization in the Arabian-Nubian shield. EGU General Assembly, held 7–12 April, 2013 in Vienna, Austria, id. EGU2013-9893.

Botros, N.S., 2004. A new classification of the gold deposits of Egypt. Ore Geol. Rev. 25, 1–37.

Cordell, L., Grauch, V.J.S., 1985. Mapping basement magnetization zones from aeromagnetic data in the San Juan Basin, New Mexico, in: Hinze, W.J. (Ed.), The Utility of Regional Gravity and Magnetic Maps: Society of Exploration Geophysicists, p. 181–197.

Cooper, G.R.J., Cowan, D.R., 2008. Edge enhancement of potential-field data using normalized statistics. Geophysics 73 (3), H1–H4.

Conoco, Inc., 1987. The Egyptian General Petroleum Corporation. Geological Map of Egypt 1:500 000, Conoco Inc.

Charbonneau, B.W., Holman, P.B., Hetu, R.J., Mac Queen, 1997. Airborne gamma spectrometer magnetic-VLF survey of northeastern Alberta, Exploring for Minerals in Alberta: Geological Survey of Canada Geoscience Contributions, Geological Survey of Canada Bulletin, vol. 500. Canada-Alberta Agreement on Mineral Development, pp. 107–132.

Core, D., Buckingham, A., Belfield, S., 2009. Detailed structural analysis of magnetic data — done quickly and objectively, SGEG Newsletter.

Cooper, G.R.J., 2003. Feature detection using sun shading. Comput. Geosci. 29 (8), 941–948.

Darnley, A.G., Ford, K.L., Garland, G.D., 1989. Regional airborne gamma-ray surveys: a review, in: Proceedings of Exploration ' 87: Third Decennial International Conference on Geophysical and Geochemical Exploration for Minerals and Groundwater, 1989. Geological Survey of Canada, special vol. 3, pp. 960.

El-Mezayen, A.M., Hassaan, M.M., El-Hadad, M., Hassanein, M.M., 1995. Petrography, geochemistry and ore microscopy of Abu Marawat metavolcanics and associated gold mineralization, North Eastern Desert, Egypt. Bull. Fac. Sci. Al-Azhar Univ. 6 (2), 1999–2021.

El-Sadek, M.A., Ammar, A.A., Sabry, A.M., 2002. Aeroradiospectrometry in the lithological mapping and environmental monitoring of Wadi Araba area. Arab. J. Sci. Eng. 27 (2A), 131–148.

El Ramly, M.F., Ivaanov, S.S., Kochin, G.C., 1970. The occurrence of gold in the Eastern Desert of Egypt Studies on Some Mineral Deposits of Egypt. Part I, Sec. A, Metallic Minerals, 21. Geol. Survey Egypt 1970, 1–22.

El-Magd, I.A., Mohy, H., Basta, F., 2015. Application of remote sensing for gold exploration in the Fawakhir area, Central Eastern Desert of Egypt. Arab. J. Geosci. 8 (6), 3523–3536.

EI-Meliegy, M.A., El-Shayeb, H.M., Meleik, M.L., Abdel-Raheim, R.M., 2000. Surface Delineation of Lithologies and Nomalies, Wadi Dib Area, Eastern Desert, Egypt, Using Aeroradiospectrometric Survey Data. Sci. J. Fac Sci. Minufiya Univ., VoL XIC: 179–231.

El Gaby, S., Greiling, R.O. (Eds.), 1988. The Pan-African Belt of Northeast Africa and Adjacent Areas. F. Vieweg, Braunschweig, pp. 369.

Elawadi, E., Ammar, A., Elsirafy, A., 2004. Mapping surface geology using airborne gamma-ray spectrometric survey data – A Case Study Proceedings of the 7th SEGJ International Symposium, Japan, November 24–26, 2004.

Feebrey, C.A., Hishida, H., Yoshioka, K., Nakayama, K., 1998. Geophysical expression of low sulfidation epithermal Au–Ag deposits and exploration implications-examples from the Hokusatsu region of SW Kyushu. Jpn. Resour. Geol. 48, 75–86.

Graham, D.F., 1993. Airborne radiometric data a tool for reconnaissance geological mapping using a GIS Thematic Conference. In: Proceedings, 9th, Geologic Remote Sensing, vol. 1, Pasadena, CA, February 8–11, 1993, pp. 43–54.

Gass, I.G., 1977. The evolution of the Pan-African crystalline basement in NE Africa and Arabia. J. Geol. Soc. London 134, 129–138.

Holden, E.J., Dentith, M., Kovesi, P., 2008. Towards the automatic analysis of regional aeromagnetic data to identify regions prospective for gold deposits. Comput. Geosci. 34, 1505–1513.

Habib, M.E., 1987. Arc-ophiolites in the Pan-African basement between Meatiq and Abu Furad, Eastern Desert, Egypt. Bull. Fac. Sci. Assiut. Univ. 16 (1), 241–283.

Hoover, D.B., Heran, W.D., Hill, P.L., 1992. The geophysical expression of selected mineral deposit models. U.S. Geological Survey Open-File report 92–557, 129p.

Irvine, R.J., Smith, M.J., 1990. Geophysical exploration for epithermal gold deposits. J. Geochem. Explor. 36, 375–412.

Jaques, A.L., Wellman, P., Whitaker, A., Wyborn, D., 1997. High-resolution geophysics in modern geological mapping. AGSO J. Aust. Geol. Geophys. 17, 159–173.
Miller, H.G., Singh, V., 1994. Potential field tilt-a new concept for location of potential field sources. J. Appl. Geophys. 32, 213–217.
Macnae, J., 1995. Applications of geophysics for the detection and exploration of kimberlites and lamproites. In: Griffin, W.L. (Ed.), Diamond Exploration into the 21st Century. Journal of Geochemical Exploration, pp. 213–243.
Morrell, A.E., Locke, C.A., Cassidy, J., Mauk, J.L., 2011. Geophysical characteristics of adularia-sericite epithermal gold-silver deposits in the Waihi-Waitekauri region New Zealand. Econ. Geol. 106, 1031–1041.
Nabighian, M.N., 1984. Toward a three-dimensional automatic interpretation of potential field data via generalized Hilbert transforms: fundamental relations. Geophysics 49 (6), 780–786.
Nigm, A.A., Khameis, A.A., 2009. Utilizing the Airborne Gamma-Ray Spectrometric data In mapping the contact zone between the Precambrian and Phanerozoic rocks at North Gabal El Shallul area, Central Eastern Desert, Egypt. NRIAG J. Astron. Geophys. Spec. Issue 143–167.
Ostrovskiy, E.A., 1975. Antagonism of radioactive elements in wallrock alteration fields and its use in aerogamma spectrometric prospecting. Int. Geol. Rev. 17 (4), 461–468.
Osman, A., Taman, Z., 1996. The genetic significance of gold-bearing sulfides from Atalla gold mine. Ann. Meeting of the Mineral Soc Egypt, Cairo (Abstract).
Portnov, A.M., 1987. Specialization of rocks toward potassium and thorium in relation to mineralization. Int. Geol. Rev. 29, 326–344.
Patra, I., Srinivas, D., Tripathi, S., Patel, A.K., 2016. High resolution Airborne Gamma ray Spectrometric data in Geological mapping-A case study from parts of Shillong Basin, Meghalaya. J. Geophys. V 3, 173–178.
Roest, W.R., Verhoef, J., Pilkington, M., 1992. Magnetic interpretation using 3-D analytic signal. Geophysics 57, 116–125.
Shives, R.B.K., Charbonneau, B.K., Ford, K.L., 1997. The detection of potassic alteration by gamma ray recognition of alteration related to mineralization, in: Exploration 97, Fourth Decennial Intern. Conf. Mineral Exploration (Toronto, Canada), p. 345–353.
Shackleton, R.M., Ries, A.C., Graham, R.H., Fitches, W.R., 1980. Late Precambrian ophiolitic mélange in the Eastern Desert of Egypt. Nature 285 (5765), 472–474.
Telford, W. M., Geldart, L. P., Sheriff, R. E., 1990. Applied Geophysics. Cambridge.
Wemegah, D.D., Preko, K., Noye, R.M., Boadi, B., Menyeh, A., Danuor, S.K., Amenyoh, T., 2015. Geophysical interpretation of possible gold mineralization zones in Kyerano, South-Western Ghana using aeromagnetic and radiometric datasets. J. Geosci. Environ. Prot. 2015 (3), 67–82.
Wijns, C., Perez, C., Kowalczyk, P., 2005. Theta map: edge detection in magnetic data. Geophysics 70 (4), L39–L43.
Youssef, M.A.S., Elkhodary, S.T., 2013. Utilization of airborne gamma ray spectrometric data for geological mapping, radioactive mineral exploration and environmental monitoring of southeastern Aswan city, South Eastern Desert, Egypt. Geophys. J. Int. 195, 1689–1700.